Detection and Location of High Impedance Faults in Multiconductor Overhead Distribution Lines Using Power Line Communication Devices

Apostolos N. Milioudis, *Student Member, IEEE,* Georgios T. Andreou, *Member, IEEE,* and Dimitris P. Labridis, *Senior Member, IEEE*

***Abstract*—An effective power system protection scheme has to be able to detect and locate all occurring faults corresponding to low and high impedance values. The latter category poses the greatest challenge for the protection schemes due to the low values of the related fault current. This paper extends previous work by the authors on the subject, aiming to achieve detection and location of high impedance faults (HIFs) in multiconductor overhead distribution networks utilizing power line communication (PLC) devices. Fault detection is proposed to be performed by a PLC device installed at the starting point of the monitored line and by using differences to the values of metrics related to input impedance at frequencies utilized by narrowband systems. Moreover, fault location can be derived by a response to impulse injection procedure utilized by all installed PLC devices along the line. The method is evaluated and validated in various simulation test cases concerning its ability to effectively detect and locate HIFs.**

***Index Terms*—Fault location, high impedance fault (HIF) detection, multiconductor distribution lines, power distribution faults, power line communications (PLCs), power system protection, smart grids.**

I. Introduction

POWER SYSTEM protection is a critical issue for both operational and safety reasons. An efficient protection scheme has to be able to ensure that the power system operates adequately, and protects the equipment as well as the public from hazardous overvoltages. For most occurring faults, overcurrent relays installed for distribution system protection can detect and cut off the supply to the feeder containing the fault. Nevertheless, the possibility of a fault occurrence that will cause a slight increase to the line current, cause of its high impedance, and thus not be detectable by the conventional protection schemes has to be taken into account. This will result to the design of an enhanced protection scheme which will be able to detect and isolate both low and high impedance faults (HIFs), improving thus the protection capability of the power system.

Manuscript received December 14, 2013; revised May 24, 2014 and September 16, 2014; accepted October 20, 2014. Date of publication November 12, 2014; date of current version February 16, 2015. Paper no. TSG-00914-2013.

The authors are with the Department of Electrical and Computer Engineering, Aristotle University of Thessaloniki, Thessaloniki 54124, Greece (e-mail: amilioud@auth.gr; gandreou@auth.gr; labridis@auth.gr).

Color versions of one or more of the figures in this paper are available online at http://ieeexplore.ieee.org.

Digital Object Identifier 10.1109/TSG.2014.2365855

The problem of HIF detection has been documented for the first time by Aucoin and Russell [1] who proposed the usage of the measured current harmonic content from 2 to 10 kHz. Since then the specific subject has drawn the attention of the scientific community and rigorous studies have been conducted toward the design of an efficient protection scheme. Lee and Osborn [2] proposed the monitoring of the zero sequence current component with respect to the value of the phase current adopting the context used in ground overcurrent relays. Moreover, artificial intelligence methods have been used such as neural networks [3], [4], fuzzy logic [5], and decision trees [6]. Additionally, Zamora *et al.* [7], [8] proposed the injection of low frequency test signals, while the utilization of wavelet transformation has also been adopted in [9]–[11].

The problem with most proposed solutions is the need for respective investments in order to incorporate them in the grid. However, the upcoming evolution of traditional power systems to smart grids may come as a solution, introducing smart grid equipment that may also be used to provide protection functionality. Most of the new capabilities of the smart grid require data communication and several technologies appear as candidates for that purpose [12]–[15]. Among them power line communications (PLC) systems, while providing narrowband [16], [17] and broadband solutions [18]–[20], also exhibit a techno-economic advantage, as they do not require further investments for network installation by utilizing the electrical grid as communication backbone. In order to improve its potential, PLC technology faces the challenge to enable additional functionality, besides data communication [21]–[25]. Within this context PLC systems could be also used to improve the power system protection schemes.

Milioudis *et al.* [26]–[29] have already investigated the possibility of utilizing PLC systems for fault detection and location in medium voltage (MV), regarding them as single conductor systems. Thus, the proposed protection scheme is the extension of that previously published work. While using the same basic conceptual schemes, monitoring differences in input impedance values at specific frequencies for fault detection and implementing response to impulse injection procedure for fault location, the initial simplification of single phase systems is no longer adopted. The protection scheme is extended to be able to take into account multiconductor configurations,

thus is capable of being applied to an entirely different configuration which poses different challenges. These extensions cannot be regarded as obvious due to the extent of differences among the single and multiconductor configurations and on the occurring underlying phenomena. The presence of multiple conductors causes coupling to the electric quantities among phases and the effect to the proposed scheme is rigorously examined. The use of specific detection and location metrics, adjusted to the special characteristics of the studied case, is proposed. Moreover, a PLC system architecture enabling the implementation of the proposed protection scheme is presented and analyzed.

II. Recommended PLC System Architecture

The detection of HIF occurrence, as shown in [28], prerequisites the isolation of the MV part of the network from the low voltage (LV) so as to avoid the effects of the constant load change on the protection system. The MV network topology is almost always static to protect the equipment from damages and every change to this status is previously known. Its static characteristic is essential for the application of the proposed method, which identifies every unexpected change to the input impedance value of the monitored topology at specific frequencies as a fault occurrence indication. Furthermore, the open ended terminations of the MV lines create standing wave phenomena on the distribution lines. These standing waves enable the HIF occurrence detection, by the use of high frequencies traditionally utilized by PLC systems for communication purposes, as was rigorously explained in [28]. Conclusively, the application of the proposed method requires the MV network to be isolated from the constantly changing LV network and the corresponding lines to be terminated to open circuits for the generation of standing waves.

High frequency performance of distribution MV to LV transformers has attracted intense research interest throughout several years. It has been shown that the transformer impedance can vary from low to high values depending on the applied frequencies [30]–[35]. This performance can determine the attenuation of a signal passing through different voltage levels resulting in feasible or infeasible transmission depending on each distribution transformers characteristics. A vast number of transformers with different high frequency performance are installed at MV distribution lines, hence the frequencies at which they exhibit high impedance values differ from case to case, therefore these could be different from the best performing frequencies that would ideally be utilized for HIF detection occurrence. Consequently, the installation of filters blocking specific selected frequencies at the transformers installation points, along with base nodes installation for LV smart meter data aggregation [36], could provide the necessary conditions for the utilization of the proposed method, as shown in Fig. 1. The installation of these band-stop filters, blocking all European Committee for Electrotechnical Standardization A frequency band, would provide the necessary standing wave production on the MV distribution lines. A few number of frequencies could be chosen for fault detection and therefore be excluded from their usage for data communication purposes by the application of masking technique [20], [37], [38]. Moreover, within the context of the suggested architecture the data communication between different voltage levels can be achieved with bypass cables [39] or WiFi connections [40], hence the only frequencies that will be blocked between MV and LV side of the transformers are the chosen frequencies that can perform best to provide fault occurrence.

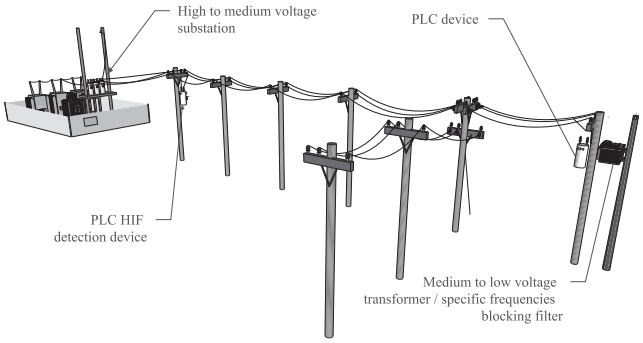

Fig. 1. Suggested PLC system architecture.

III. Theoretical Formulation

The proposed protection system aims to address both fault detection and location. The former is suggested to be achieved by monitoring deviations to the values of the arrangement's input impedance at frequencies used by narrowband PLC systems while the latter is addressed by the utilization of the differences that occur at the network responses to impulse injections as measured by installed PLC devices along the line [28], [29]. The next section deals with the calculation of the input impedance and responses to impulse injections in multiconductor arrangements under normal operational conditions and after a fault occurrence.

A. Detection of HIF Occurrence

1) Input Impedance of Multiconductor Transmission Line Segment With No Lateral Branches: Let us consider a multiconductor transmission line comprised of N conductors above the ground plane. Its per unit length (pul) electrical characteristics are represented through $N \times N$ matrices $\mathbf{Z}'$ and $\mathbf{Y}'$, which correspond to the pul impedance and admittance matrix, respectively. The analysis of the multiconductor transmission line can be simplified implementing the modal transformation technique, through which only N independent modes may be considered. Through the modal approach the diagonal matrix γ, characteristic impedance matrix $\mathbf{Z_c}$ and characteristic admittance matrix $\mathbf{Y_c}$ and voltage transformation matrix $\mathbf{T_V}$ can be calculated as shown in [41].

Considering a multiconductor transmission line segment of length l that is terminated to a load with an impedance matrix $\mathbf{Z_L}$, it is known that at the termination point the voltage reflection coefficient matrix, $\Gamma_{\mathbf{V}}(0)$, can be calculated using (1). Furthermore, the voltage reflection coefficient matrix, $\Gamma_{\mathbf{V}}(l)$, which corresponds to the starting point of the transmission line segment can be computed

$$\Gamma_{\mathbf{V}}(0) = [\mathbf{Z_L} - \mathbf{Z_c}] \cdot [\mathbf{Z_L} + \mathbf{Z_c}]^{-1} \quad (1)$$

$$\Gamma_{\mathbf{V}}(l) = \mathbf{T_V} \cdot e^{-\gamma l} \cdot \mathbf{T_V}^{-1} \cdot \Gamma_{\mathbf{V}}(0) \cdot \mathbf{T_V} e^{-\gamma l} \cdot \mathbf{T_V}^{-1}. \quad (2)$$

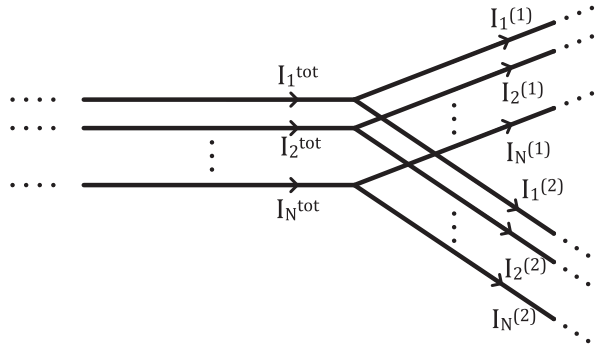

Fig. 2. Junction point.

In general, the input impedance matrix at an arbitrary point x of the total length is given by (3), as explained in [41]

$$\mathbf{Z}_{\text{in}}(x) = \mathbf{Z_c} \cdot [\mathbf{I_N} + \mathbf{Y_c} \cdot \Gamma_{\mathbf{V}}(x) \cdot \mathbf{Z_c}] \cdot [\mathbf{I_N} - \mathbf{Y_c} \cdot \Gamma_{\mathbf{V}}(x) \cdot \mathbf{Z_c}]^{-1} \tag{3}$$

where $\mathbf{I_N}$ is the $N \times N$ identity matrix.

The total length of the line segment has to be considered for the calculation of total input impedance $\mathbf{Z}_{\text{in}}$. The analytic formula for this is shown

$$\mathbf{Z}_{\text{in}} = \mathbf{Z_c} \cdot [\mathbf{I_N} + \mathbf{Y_c} \cdot \Gamma_{\mathbf{V}}(l) \cdot \mathbf{Z_c}] \cdot [\mathbf{I_N} - \mathbf{Y_c} \cdot \Gamma_{\mathbf{V}}(l) \cdot \mathbf{Z_c}]^{-1}. \tag{4}$$

2) Incorporation of Junction Points: Considering a junction point at which the multiconductor transmission line is divided into two parts (1) and (2) with input impedance matrices $\mathbf{Z}_{\text{in}}^{(1)}$ and $\mathbf{Z}_{\text{in}}^{(2)}$ respectively, the Kirchhoff's junction rule can be applied. In more detail, the total current vector $\mathbf{I}^{\text{tot}}$ is equal to the sum of current vectors that correspond to each part of the transmission line, $\mathbf{I}^{(1)}$ and $\mathbf{I}^{(2)}$, as shown in Fig. 2

$$\mathbf{I}^{\text{tot}} = \underbrace{\mathbf{Z}_{\text{in}}^{(1)^{-1}} \cdot \mathbf{V}}_{\mathbf{I}^{(1)}} + \underbrace{\mathbf{Z}_{\text{in}}^{(2)^{-1}} \cdot \mathbf{V}}_{\mathbf{I}^{(2)}}. \tag{5}$$

Hence, the apparent impedance matrix $\mathbf{Z_{eq}}$ corresponding to the parallel connection of two transmission line segments at the junction point, which can be used as a termination matrix ($\mathbf{Z_L}$) for the rest of the transmission line in (1), can be calculated through

$$\mathbf{Z_{eq}} = \left[\mathbf{Z}_{\text{in}}^{(1)^{-1}} + \mathbf{Z}_{\text{in}}^{(2)^{-1}}\right]^{-1}. \tag{6}$$

3) Incorporation of Fault Location Points: Let us now consider that a single phase HIF of Z_{fault} resistance occurs at phase P, corresponding to a admittance matrix $\mathbf{Y_f}$, where its elements are given as explained

$$Y_{f_{ij}} = \begin{cases} \frac{1}{Z_{\text{fault}}} & \text{if } i = P, \text{ and if } i = j \\ 0 & \text{for all other cases.} \end{cases} \tag{7}$$

The input impedance matrix of the transmission line segment just after the fault location is represented as $\mathbf{Z}$, the voltage vector $\mathbf{V}$, and the current vector corresponding to the point just before the fault location is $\mathbf{I}^{\text{tot}}$. Applying the Kirchhoff's junction rule at the point of the fault occurrence, as explained before, gives (8). The apparent impedance matrix, which can be used as a termination matrix ($\mathbf{Z_L}$) for the rest of the transmission line in (1), can be computed

$$\mathbf{I}^{\text{tot}} = \mathbf{Z}^{-1} \cdot \mathbf{V} + \mathbf{Y_f} \cdot \mathbf{V} \tag{8}$$

$$\mathbf{Z_{eq}} = \left(\mathbf{Z}^{-1} + \mathbf{Y_f}\right)^{-1}. \tag{9}$$

The case of broken conductor fault requires a slightly different approach. Specifically, the elements of the apparent impedance matrix $\mathbf{Z_{eq}}$ elements are defined

$$Z_{eq_{ij}} = \begin{cases} Z_{\text{fault}} & \text{if } i = P, \text{ and if } i = j \\ Z_{ij} & \text{for all other cases} \end{cases} \tag{10}$$

where Z_{ij} correspond to the elements of impedance matrix $\mathbf{Z}$.

4) HIF Detection Metrics: The overall input impedance calculation can be performed adopting the procedure introduced in [28]. Under normal operational conditions the corresponding input impedance matrix is denoted as $\mathbf{Z}_{\text{in}}$, whereas during the occurrence of a HIF it is denoted as $\mathbf{Z}_{\text{infault}}$. The fault detection can be achieved through the deviations to the values of input impedance matrix elements due to the fault occurrence, derived from input voltage and current measurements.

Two metrics can be used for fault detection, i.e., functions $\mathbf{D_p}$ and $\mathbf{D_{ep}}$ as they are defined

$$\mathbf{D_p} = \begin{bmatrix} \frac{|Z^{\text{app}}_{\text{in\_fault1}}(f)| - |Z^{\text{app}}_{\text{in\_1}}(f)|}{|Z^{\text{app}}_{\text{in\_1}}(f)|} \\ \frac{|Z^{\text{app}}_{\text{in\_fault2}}(f)| - |Z^{\text{app}}_{\text{in\_2}}(f)|}{|Z^{\text{app}}_{\text{in\_2}}(f)|} \\ \vdots \\ \frac{|Z^{\text{app}}_{\text{in\_faultN}}(f)| - |Z^{\text{app}}_{\text{in\_N}}(f)|}{|Z^{\text{app}}_{\text{in\_N}}(f)|} \end{bmatrix} \cdot 100\% \tag{11}$$

$$\mathbf{D_{ep}}(i,j) = \frac{\left|Z_{\text{infault}_{ij}}(f)\right| - \left|Z_{\text{in}_{ij}}(f)\right|}{\left|Z_{\text{in}_{ij}}(f)\right|} \cdot 100\% \tag{12}$$

where $Z^{\text{app}}_{\text{in\_fault}i}(f)$ (apparent input impedance of phase i) is equal to $(V_{\text{in}i}(f))/(I_{\text{in}i}(f))$, with $V_{\text{in}i}(f)$ and $I_{\text{in}i}(f)$ being the input voltage and current of phase i under fault occurrence, while $Z^{\text{app}}_{\text{in\_}i}(f)$ corresponds to the same under normal operational conditions. Moreover, $Z_{\text{infault}}(i,j)$ is the ij element of input impedance matrix $\mathbf{Z}_{\text{infault}}$, while $Z_{\text{in}}(i,j)$ corresponds to the ij element of input impedance matrix $\mathbf{Z}_{\text{in}}$. In more detail, functions $\mathbf{D_p}$ and $\mathbf{D_{ep}}$ correspond to a $N \times 1$ vector and a $N \times N$ matrix for each studied frequency f, respectively.

B. Location of HIF Position

Following the procedure described in [29] and [42], the location of the fault can be derived after the fault detection by the implementation of a test signal injection sequence by installed PLC devices along the length of the monitored distribution line. These PLC devices could be responsible for narrowband or broadband data communication and can be used for the location of the fault, which will always occur among two successively installed devices. The location can be computed through the responses to impulse injections measured by both devices adjacent to the fault point. The injection of a test impulse by each installed PLC device under fault conditions

will result to altered responses, as compared to those under normal operational conditions. These alterations can be used for the exact fault location.

Considering an impulse as an input, the corresponding input voltage vector is $\mathbf{V}_{\text{in}}(f)$, and its elements are equal to unity due to the impulse Fourier transform. The voltage vector at every point of the line, $\mathbf{V}(f)$, can be computed through the utilization of the transfer function matrix $\mathbf{H}(f)$, as in (13), where f corresponds to the studied frequency. The response to impulse injection in time domain, $\mathbf{h}(t)$, corresponding to a $N \times 1$ vector of time domain signals can be computed using the inverse fast Fourier transform (IFFT)

$$\mathbf{V}(f) = \mathbf{H}(f) \cdot \mathbf{V}_{\text{in}}(f) \tag{13}$$

$$\mathbf{V}(f) \xrightarrow{\text{IFFT}} \mathbf{h}(t). \tag{14}$$

For the extension of the adopted methodology for transfer function calculations in [29], the reflection and transmission coefficients for multiconductor arrangements at various cases have to be defined. If a pulse is traveling over a distribution line segment of characteristic impedance matrix $\mathbf{Z_c}$ toward a junction point at which two line segments with characteristic impedance matrices $\mathbf{Z_{ci}}$ and $\mathbf{Z_{cj}}$ are connected, the voltage reflection and transmission coefficients at the junction point are computed as shown

$$\Gamma_{\mathbf{V}} = \left(\mathbf{Z_c}^{-1} + \mathbf{Z_{ci}}^{-1} + \mathbf{Z_{cj}}^{-1}\right)^{-1} \times \left(\mathbf{Z_c}^{-1} - \mathbf{Z_{ci}}^{-1} - \mathbf{Z_{cj}}^{-1}\right) \tag{15}$$

$$\mathbf{T_V} = \mathbf{1_n} + \Gamma_{\mathbf{V}}. \tag{16}$$

Similarly, the voltage reflection coefficient at the point that the fault occurs is defined

$$\Gamma_{\mathbf{V}} = \left(\mathbf{Z_c}^{-1} + \mathbf{Y_f} + \mathbf{Z_{ci}}^{-1}\right)^{-1} \cdot \left(\mathbf{Z_c}^{-1} - \mathbf{Y_f} - \mathbf{Z_{ci}}^{-1}\right) \tag{17}$$

where $\mathbf{Z_{ci}}$ is the characteristic impedance matrix of the line segment toward which the pulse is traveling. Moreover, the voltage reflection coefficient at a termination point can be computed

$$\Gamma_{\mathbf{V}} = \left(\mathbf{Z_c}^{-1} + \mathbf{Z_L}^{-1}\right)^{-1} \cdot \left(\mathbf{Z_c}^{-1} - \mathbf{Z_L}^{-1}\right). \tag{18}$$

Using the coefficients as they have been defined, the process described in [29] and [42] can be adopted for response to impulse injection calculations at the two PLC devices installed bilaterally and closest to the fault point, with the only difference that scalars used for the single phase approach will be transformed to vectors and matrices accordingly for the multiconductor approach.

The fault occurrence leads to topology change and thus to the differentiation of network responses, as they can be measured by installed PLC devices along the line. Hence, fault location can be derived through these deviations. Considering the devices installed bilaterally and closest to the fault location, they are denoted as Devices 1 and 2, where Device 1 is injecting and Device 2 is receiving the test impulse, while both are measuring the response. The fault location can be computed by comparing the responses between normal conditions and during fault occurrence, hence the metric shown

$$D_{ij}(t) = h_{ijn}(t) - h_{ijf}(t) \tag{19}$$

where i corresponds to the studied device, j to the studied phase, n to normal operation conditions, and f to the state during fault occurrence.

Time synchronization among communication devices is an issue of study in [24], [25], however, it is not a problem for the proposed methodology, because it relies on the fact the measured responses will be compared to stored responses corresponding to normal operational conditions. Let us assume that the test pulse is injected at time instant t_0. Knowing that and also the measurement sampling rate the measured response can be compared to the stored one by the device itself, since only the starting points time alignment of the two responses is necessary. More concretely, let us assume that the response under normal operational conditions for a device that injects the test impulses is formulated by N vectors, where N are the installed phases, of $1 \times M$size, where M is the total measuring samples corresponding to total measurement time T, where $T = M/(f_{\text{sampling}})$ and f_{sampling} is the sampling frequency. When test impulses are injected at time instant t_0 in order to determine whether a fault is near the particular device, the M following samples have to be stored for all N phases in order to be compared with the responses for normal operational conditions. Consequently, no sophisticated time synchronization technique is necessary. For Device 2, the process to achieve measurement time alignment is slightly different. For this case, Device 1 has to communicate with Device 2 and announce that it will start the impulse injecting procedure. Device 2 starts and records measurements for a predetermined time period $T^{'}$. Let us assume that the first pulses of the response measurement arrive at Device 2 at time instant t_1. This time instant has to be aligned with the time instant that corresponds to the arrival of the first pulses of the responses under normal operational conditions. This achieves perfect time alignment among responses under fault and normal operational conditions because first pulses arrive always with a time delay equal to $t = u/d = t_1 - t_0$,where u is the propagation speed, d the distance among the devices, regardless of the fault that occurs.

IV. Simulations

The aim of the conducted simulations is to evaluate the efficiency of the proposed method taking into account all factors involved. The chosen test case of a multiconductor system corresponds to a three phase overhead MV system, parameters of which are included in Table I.

A. Detection of HIF Occurrence

First, the effect of a HIF occurrence to the input impedance characteristics of various distribution line topologies is examined. The first test case corresponds to the occurrence of a 15 kΩ fault in phase 3 and 6 km far from the starting point of a 10 km line containing no branches. The absolute value of the apparent input impedance of phase 3, at which the fault occurs, versus frequency under normal operational conditions

TABLE I
THREE PHASE OVERHEAD MV SYSTEM—SIMULATION PARAMETERS

Conductor material	ACSR
Cross section (mm^2)	70/12
Height, h (m)	10
Distance among successive conductors (m)	1
Earth conductivity, σ_g (S/m)	0.01
Earth permittivity, ε_g (F/m)	$10 \cdot \varepsilon_0$
Frequency range (kHz)	3-95

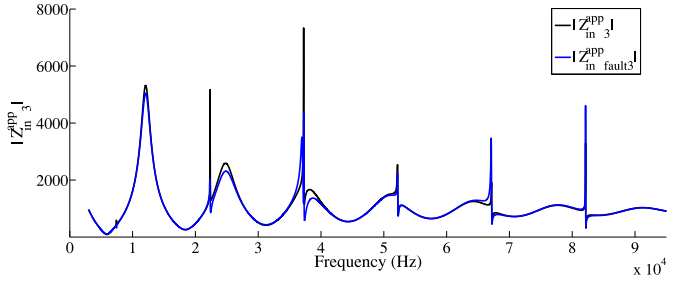

Fig. 3. Absolute value of phase 3 apparent input impedance under normal conditions ($|Z^{app}_{in\ 3}|$) and after a 15 kΩ fault occurrence in phase 3 and 6 km far from the starting point of a 10 km line ($|Z^{app}_{in\ fault3}|$).

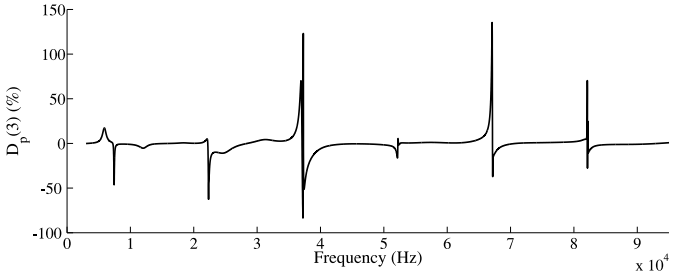

Fig. 4. Function $D_p(3)$ versus frequency for a 15 kΩ fault occurrence in phase 3 and 6 km far from the starting point of 10 km line.

and after the fault occurrence is shown in Fig. 3. Significant deviations are noticed among the two curves. The calculated percentage divergence represented by the metric $\mathbf{D_p}(3)$ is illustrated in Fig. 4. As it can be easily deducted the occurrence of the fault causes large deviations (up to more than 100 %) to the value of the apparent input impedance at specific frequencies of the studied frequency range.

For the next test case, the fault impedance is reduced to 1.5 kΩ, in order to investigate its effect to the differences caused to the values of the apparent input impedances of all three installed phases. The respective calculated results are illustrated in Fig. 5. Compared to the previous test case the deviations are considerably larger, leading to the expected conclusion that as the fault impedance value increases toward infinity, it becomes more difficult to detect the fault. Also, the significant deviations are noticed at the same frequencies for all three phases and moreover at the same frequencies of the previous test case showing that specific frequencies correspond to high deviations in impedance values, thus can be used for HIF detection for the same fault location. Furthermore, it is derived that the deviations calculated for the two phases

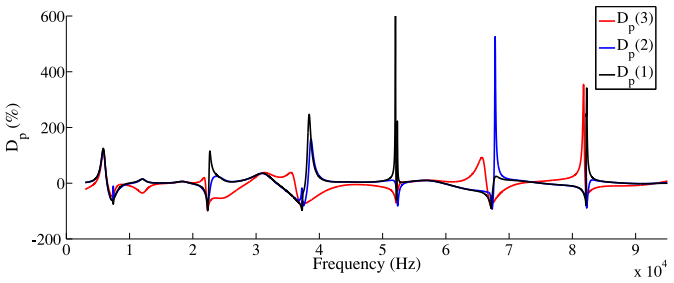

Fig. 5. Function D_p versus frequency for a 1.5 kΩ fault occurrence in phase 3 and 6 km far from the starting point of a 10 km line.

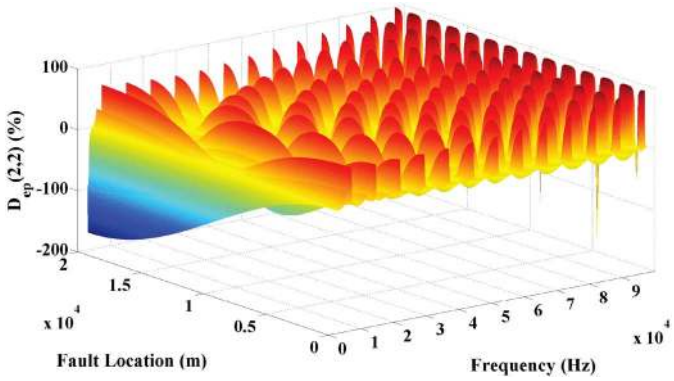

Fig. 6. Fault location effect on function $D_{ep}(2, 2)$ versus frequency for a 15 kΩ fault occurrence in phase 2 of a 20 km line.

that do not contain the fault, i.e., phases 1 and 2, are notable, due to the electromagnetic coupling that is present to multi-conductor arrangements. This indicates that it would suffice to monitor only one phase and provide effective HIF detection for all installed phases.

The effect of fault location and frequency to the values of detection metric $\mathbf{D_{ep}}(2, 2)$ is further illustrated in Fig. 6. This corresponds to the percentage deviation calculated for the $(2, 2)$th entry of the input impedance matrix among normal and fault conditions. The considered fault corresponds to 15 kΩ and occurs at phase 2 of a 20 km line without branches. It is observed that significant values of deviation up to 100 % are calculated for many frequencies, but not for the entire line length. As shown in [28], a combination of these frequencies can be utilized in order to provide efficient monitoring for the total length.

The next test case corresponds to a fault impedance of 5 kΩ at phase 3. The effect of the fault location and the selected frequency to the value of metric $\mathbf{D_p}(3)$ is presented in Fig. 7. It is deduced that the calculated deviations are much higher for the examined metric, exhibiting values of hundreds of percent. It has to be noted that the maximum value of the metric was limited to 1000 % to enhance the figure readability. Comparing the results with the previous examined case, it can be concluded that the usage of metrics corresponding to apparent input impedance deviations (i.e., metric $\mathbf{D_p}$) lead to much higher deviations, but at the same time more frequencies have to be reserved for HIF detection over the entire length of the monitored line. The same conclusions can also be derived by the examination of a 10 kΩ fault that is considered to occur

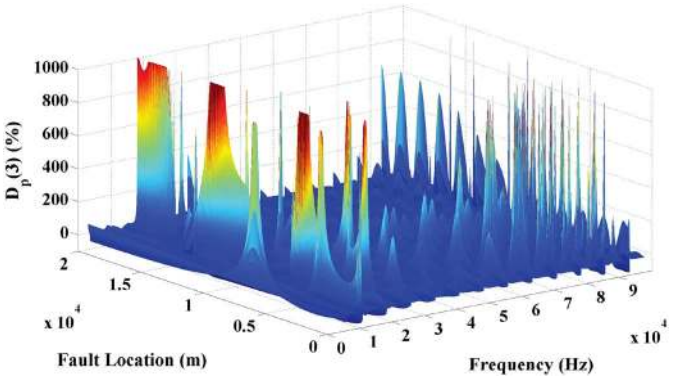

Fig. 7. Fault location effect on function $D_p(3)$ versus frequency for a 5 kΩ fault occurrence in phase 3 of a 20 km line.

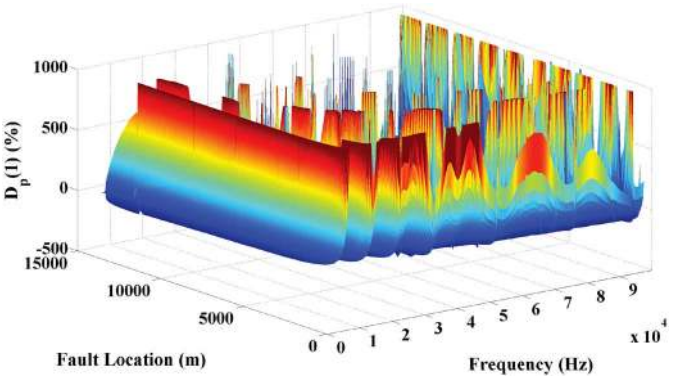

Fig. 10. Broken conductor, in phase 3 of a real topology, fault location effect on function $D_p(1)$ versus frequency.

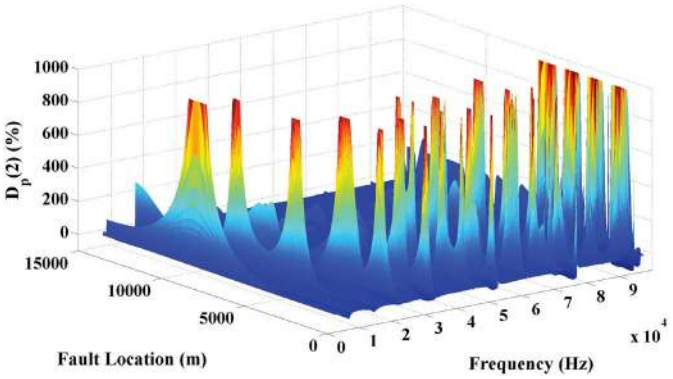

Fig. 8. Fault location effect on function $D_p(2)$ versus frequency for a 10 kΩ fault occurrence in phase 2 of a real topology.

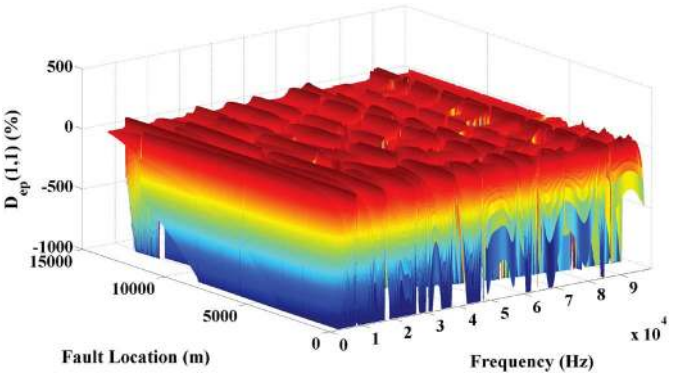

Fig. 11. Broken conductor, in phase 3 of a real topology, fault location effect on function $D_{ep}(1, 1)$ versus frequency.

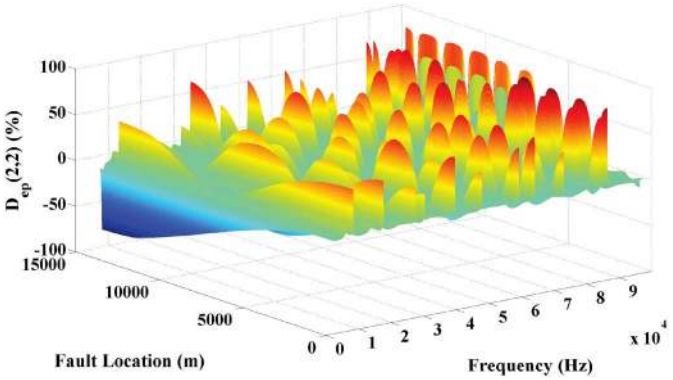

Fig. 9. Fault location effect on function $D_{ep}(2, 2)$ versus frequency for a 10 kΩ fault occurrence in phase 2 of a real topology.

at various locations of a real topology of the Greek MV distribution network as it was presented in [28]. The corresponding results for detection metrics $\mathbf{D_p}(2)$ and $\mathbf{D_{ep}}(2, 2)$ are shown in Figs. 8 and 9, respectively.

Subsequently, the case of a broken conductor occurrence along the phase 3 of the real topology is chosen to be studied. The effect of various fault locations and frequencies on metrics $\mathbf{D_p}(1)$ and $\mathbf{D_p}(1, 1)$, i.e., corresponding to a phase that does not contain the fault, is presented in Figs. 10 and 11, respectively. The illustrated deviations are considerably high for both examined cases and for a variety of frequencies denoting that the broken conductor case is easily detectable by both metrics involved in the proposed HIF detection scheme. It has to be emphasized that the metrics do not correspond to the phase at which the fault is considered to occur, thus it can be deducted that it will suffice to monitor only one phase to provide detection for all installed phases. Once again the maximum values of the metrics were limited to 1000 % to enhance the figures readability.

B. Location of HIF Position

After a fault is detected by the deviation it causes to the values of metrics associated with input impedance parameters its exact location can be derived after the application of a test impulse procedure utilizing all installed PLC devices along the monitored line as described in [29] utilizing reflection and transmission matrices calculated as described in Section III-B of this paper. The fault will always occur between two successive communication devices, therefore the analysis will focus on that segment of the network. During the test impulse procedure, one of these devices injects a test impulse into the network, while measuring at the same time the response. This is denoted as Device 1. The second device (denoted as Device 2) also measures the response to the injected impulse, as observed by it. For the purpose of this paper, the distance between these devices is considered to be equal to 1 km with no branches, corresponding to a typical distance between PLC

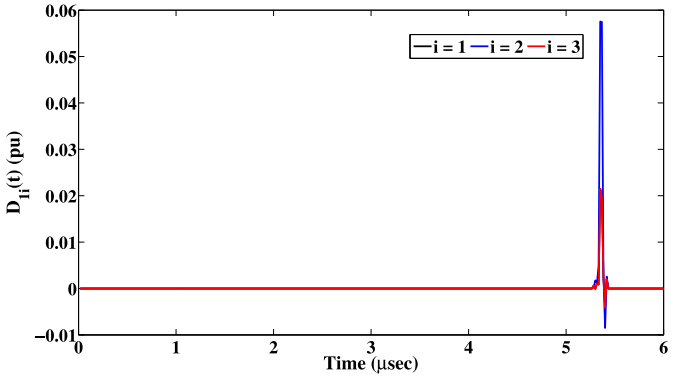

Fig. 12. Effect of a 1.5 kΩ fault located in phase 2 and at distance of 800 m from Device 1 on responses to injected impulses of all phases measured from the same device through function $D_{1i}(t)$.

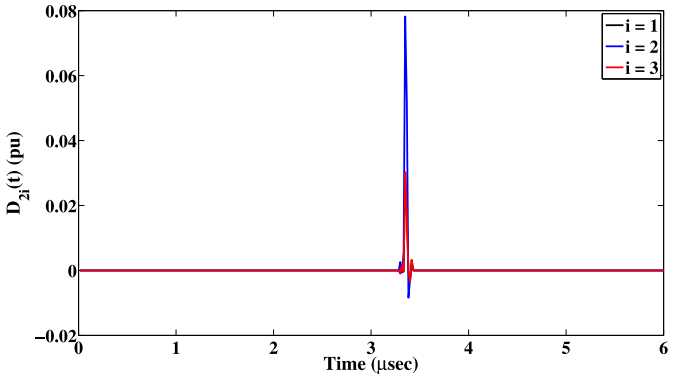

Fig. 13. Effect of a 1.5 kΩ fault located in phase 2 and at distance of 800 m from Device 1 on responses to injected impulses of all phases measured from Device 2 through function $D_{2i}(t)$.

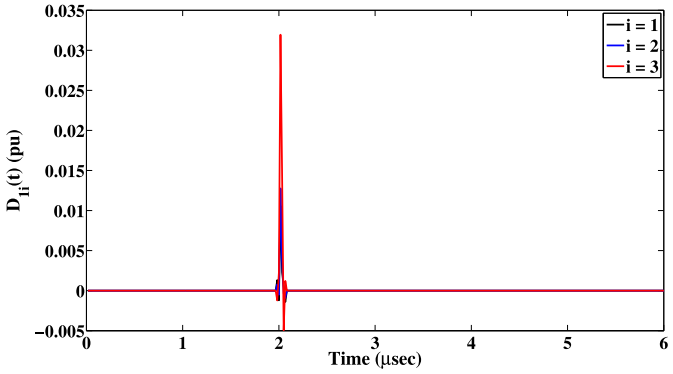

Fig. 14. Effect of a 5 kΩ fault located in phase 3 and at distance of 300 m from Device 1 on responses to injected impulses of all phases measured from the same device through function $D_{1i}(t)$.

devices in MV networks [18], [20]. Moreover, the connection points are considered to be matched.

In the first examined test case, a fault equal to 1.5 kΩ located at phase 2 and at distance of 800 m from Device 1 is considered. The effect of its occurrence to the responses of all three phases as they are measured from Devices 1 and 2 is presented in Figs. 12 and 13, respectively.

More specifically, the difference among responses of all three phases under normal operation conditions ($h_{1in}(t)$) and

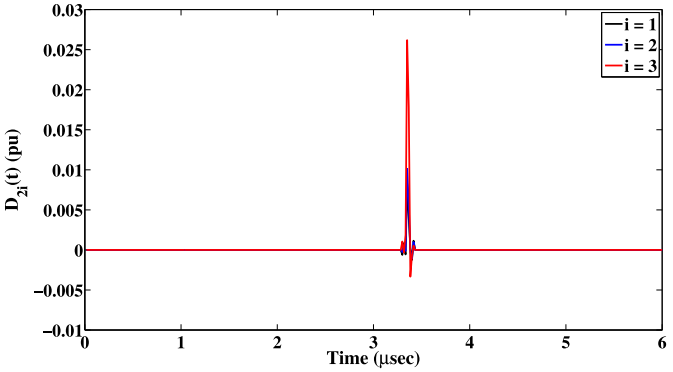

Fig. 15. Effect of a 5 kΩ fault located in phase 3 and at distance of 300 m from Device 1 on responses to injected impulses of all phases measured from Device 2 through function $D_{2i}(t)$.

the responses after the fault occurrence ($h_{1if}(t)$) are presented in Fig. 12 through $D_{1i}(t)$. The same time series are included in Fig. 13 corresponding in this case to the measured values from Device 2. It can be derived from both figures that the fault imposes differences to the responses for both devices and for all installed phases. The extra peaks measured after the fault occurrence can be used to provide exact fault location through the usage of the known propagation velocity of the impulse [29]. Moreover, these deviations are much larger for the phase containing the fault, i.e., phase 2 in the example presented here, as compared to the other phases. However, it has to be noted that, as for the fault detection case, the utilization of only one phase could provide efficient fault location for all installed conductors. Similar results and conclusions are depicted from the case investigated next, corresponding to a 5 kΩ fault, located at phase 3 and at a distance of 300 m from Device 1, as shown in Figs. 14 and 15.

V. Conclusion

In this paper, a protection scheme dealing with the detection and location of HIFs in multiconductor distribution networks is presented and evaluated. It utilizes installed PLC devices along the monitored line and takes into account the electromagnetic coupling among the multiple phase conductors. A PLC device installed at the starting point of the monitored line is suggested to be used for fault detection. The device is continuously monitoring deviations caused to detection metrics that are associated with the input impedance of the network at specific frequencies, when a fault occurs, and as compared to normal operational conditions. This can be achieved through a specific PLC system architecture that is also proposed here. The process for the calculation of the input impedance matrix of multiconductor arrangements under normal operational conditions and after the occurrence of a fault is presented. The implementation of two different detection metrics is tested and the advantages and drawbacks of each one are stated. Additionally, the proposed HIF detection approach is tested in several distribution line test cases, as well as in a real distribution topology, with satisfactory results for all examined cases. Moreover, the effect

of the fault occurrence on responses to injected impulses, as they are measured from installed PLC devices, is shown. Exact fault location can be derived by using these responses. Finally, it is shown that the installation of measuring equipment in only one phase could provide both detection and location related to all installed conductors in the examined arrangement.

REFERENCES

[1] B. Aucoin and B. Russell, "Distribution high impedance fault detection utilizing high frequency current components," *IEEE Trans. Power App. Syst.*, vol. PAS-101, no. 6, pp. 1596–1606, Jun. 1982.

[2] R. Lee and R. H. Osborn, "A microcomputer based data acquisition system for high impedance fault analysis," *IEEE Power Eng. Rev.*, vol. PER-5, no. 10, p. 35, Oct. 1985.

[3] S. Ebron, D. Lubkeman, and M. White, "A neural network approach to the detection of incipient faults on power distribution feeders," *IEEE Trans. Power Del.*, vol. 5, no. 2, pp. 905–914, Apr. 1990.

[4] J.-H. Ko, J.-C. Shim, C.-W. Ryu, C.-G. Park, and W.-Y. Yim, "Detection of high impedance faults using neural nets and chaotic degree," in *Proc. 1998 Int. Conf. Energy Manage. Power Del. (EMPD)*, vol. 2. Singapore, pp. 399–404.

[5] F. Jota and P. R. S. Jota, "High-impedance fault identification using a fuzzy reasoning system," *IEE Proc. Gener. Transmiss. Distrib.*, vol. 145, no. 6, pp. 656–661, Nov. 1998.

[6] Y. Sheng and S. Rovnyak, "Decision tree-based methodology for high impedance fault detection," *IEEE Trans. Power Del.*, vol. 19, no. 2, pp. 533–536, Apr. 2004.

[7] I. Zamora, A. Mazon, K. J. Sagastabeitia, and J. Zamora, "New method for detecting low current faults in electrical distribution systems," *IEEE Trans. Power Del.*, vol. 22, no. 4, pp. 2072–2079, Oct. 2007.

[8] J. Zamora, I. Zamora, A. Mazon, and K. J. Sagastabeitia, "Optimal frequency value to detect low current faults superposing voltage tones," *IEEE Trans. Power Del.*, vol. 23, no. 4, pp. 1773–1779, Oct. 2008.

[9] D. C. T. Wai and X. Yibin, "A novel technique for high impedance fault identification," *IEEE Trans. Power Del.*, vol. 13, no. 3, pp. 738–744, Jul. 1998.

[10] M. Michalik, W. Rebizant, M. Lukowicz, S.-J. Lee, and S.-H. Kang, "High-impedance fault detection in distribution networks with use of wavelet-based algorithm," *IEEE Trans. Power Del.*, vol. 21, no. 4, pp. 1793–1802, Oct. 2006.

[11] M. Michalik, M. Lukowicz, W. Rebizant, S.-J. Lee, and S.-H. Kang, "Verification of the wavelet-based HIF detecting algorithm performance in solidly grounded MV networks," *IEEE Trans. Power Del.*, vol. 22, no. 4, pp. 2057–2064, Oct. 2007.

[12] A. Bose, "Smart transmission grid applications and their supporting infrastructure," *IEEE Trans. Smart Grid*, vol. 1, no. 1, pp. 11–19, Jun. 2010.

[13] P. Zhang, F. Li, and N. Bhatt, "Next-generation monitoring, analysis, and control for the future smart control center," *IEEE Trans. Smart Grid*, vol. 1, no. 2, pp. 186–192, Sep. 2010.

[14] F. Li *et al.*, "Smart transmission grid: Vision and framework," *IEEE Trans. Smart Grid*, vol. 1, no. 2, pp. 168–177, Sep. 2010.

[15] G. Heydt, "The next generation of power distribution systems," *IEEE Trans. Smart Grid*, vol. 1, no. 3, pp. 225–235, Dec. 2010.

[16] T. Papadopoulos, C. Kaloudas, A. Chrysochos, and G. Papagiannis, "Application of narrowband power-line communication in medium-voltage smart distribution grids," *IEEE Trans. Power Del.*, vol. 28, no. 2, pp. 981–988, Apr. 2013.

[17] T. A. Papadopoulos, A. I. Chrysochos, and G. K. Papagiannis, "Narrowband power line communication: Medium voltage cable modeling and laboratory experimental results," *Elect. Power Syst. Res.*, vol. 102, pp. 50–60, Sep. 2013.

[18] P. Amirshahi and M. Kavehrad, "High-frequency characteristics of overhead multiconductor power lines for broadband communications," *IEEE J. Sel. Areas Commun.*, vol. 24, no. 7, pp. 1292–1303, Jul. 2006.

[19] J. Anatory, N. Theethayi, R. Thottappillil, M. Kissaka, and N. Mvungi, "Broadband power-line communications: The channel capacity analysis," *IEEE Trans. Power Del.*, vol. 23, no. 1, pp. 164–170, Jan. 2008.

[20] A. Lazaropoulos and P. Cottis, "Capacity of overhead medium voltage power line communication channels," *IEEE Trans. Power Del.*, vol. 25, no. 2, pp. 723–733, Apr. 2010.

[21] S. Galli, A. Scaglione, and Z. Wang, "For the grid and through the grid: The role of power line communications in the smart grid," *Proc. IEEE*, vol. 99, no. 6, pp. 998–1027, Jun. 2011.

[22] V. Taylor and M. Faulkner, "Line monitoring and fault location using spread spectrum on power line carrier," *IEE Proc. Gener. Transmiss. Distrib.*, vol. 143, no. 5, pp. 427–434, Sep. 1996.

[23] P. A. A. F. Wouters, P. C. J. M. van der Wielen, J. Veen, P. Wagenaars, and E. Steennis, "Effect of cable load impedance on coupling schemes for MV power line communication," *IEEE Trans. Power Del.*, vol. 20, no. 2, pp. 638–645, Apr. 2005.

[24] T. Erseghe, S. Tomasin, and A. Vigato, "Topology estimation for smart micro grids via powerline communications," *IEEE Trans. Signal Process.*, vol. 61, no. 13, pp. 3368–3377, Jul. 2013.

[25] M. Ahmed and L. Lampe, "Power line communications for low-voltage power grid tomography," *IEEE Trans. Commun.*, vol. 61, no. 12, pp. 5163–5175, Dec. 2013.

[26] A. Milioudis, G. Andreou, and D. Labridis, "High impedance fault detection using power line communication techniques," in *Proc. 2010 45th Int. Univ. Power Eng. Conf. (UPEC)*, Cardiff, U.K., pp. 1–6.

[27] A. Milioudis, G. Andreou, and D. Labridis, "High impedance fault evaluation using narrowband power line communication techniques," in *Proc. 2011 IEEE Trondheim PowerTech*, Trondheim, Norway, pp. 1–6.

[28] A. Milioudis, G. Andreou, and D. Labridis, "Enhanced protection scheme for smart grids using power line communications techniques—Part I: Detection of high impedance fault occurrence," *IEEE Trans. Smart Grid*, vol. 3, no. 4, pp. 1621–1630, Dec. 2012.

[29] A. Milioudis, G. Andreou, and D. Labridis, "Enhanced protection scheme for smart grids using power line communications techniques—Part II: Location of high impedance fault position," *IEEE Trans. Smart Grid*, vol. 3, no. 4, pp. 1631–1640, Dec. 2012.

[30] S. Chimklai and J. Marti, "Simplified three-phase transformer model for electromagnetic transient studies," *IEEE Trans. Power Del.*, vol. 10, no. 3, pp. 1316–1325, Jul. 1995.

[31] A. Cataliotti, V. Cosentino, D. Di Cara, and G. Tine, "Oil-filled MV/LV power-transformer behavior in narrow-band power-line communication systems," *IEEE Trans. Instrum. Meas.*, vol. 61, no. 10, pp. 2642–2652, Oct. 2012.

[32] A. Cataliotti, D. Di Cara, R. Fiorelli, and G. Tine, "Power-line communication in medium-voltage system: Simulation model and onfield experimental tests," *IEEE Trans. Power Del.*, vol. 27, no. 1, pp. 62–69, Jan. 2012.

[33] A. Sendin, A. Llano, A. Arzuaga, and I. Berganza, "Strategies for PLC signal injection in electricity distribution grid transformers," in *Proc. IEEE Int. Symp. Power Line Commun. Appl. (ISPLC)*, Udine, Italy, Apr. 2011, pp. 346–351.

[34] T. Tran-Anh, P. Auriol, and T. Tran-Quoc, "High frequency power transformer modeling for power line communication applications," in *Proc. IEEE PES Power Syst. Conf. Expo. (PSCE)*, Atlanta, GA, USA, Oct. 2006, pp. 1069–1074.

[35] G. Artale *et al.*, "Medium voltage smart grid: Experimental analysis of secondary substation narrow band power line communication," *IEEE Trans. Instrum. Meas.*, vol. 62, no. 9, pp. 2391–2398, Sep. 2013.

[36] T. Borsche, F. Oldewurtel, and G. Andersson, "Minimizing communication cost for demand response using state estimation," in *Proc. IEEE Grenoble PowerTech (POWERTECH),* Grenoble, France, Jun. 2013, pp. 1–6.

[37] P. Achaichia, M. Le Bot, and P. Siohan, "Potential impact of the CENELEC spectral mask on broadband PLC networks," in *Proc. 17th IEEE Int. Symp. Power Line Commun. Appl. (ISPLC)*, Johannesburg, South Africa, Mar. 2013, pp. 7–12.

[38] P. Torio and M. Sanchez, "Eliminating man-made noise from PLC systems by taking advantage of the masked tones," in *Proc. IEEE Int. Symp. Electromagn. Compat. (EMC)*, Pittsburgh, PA, USA, Aug. 2012, pp. 744–748.

[39] C. Kikkert, "MV to LV transformer PLC bypass coupling networks for a low cost smart grid rollout," in *Proc. 2011 IEEE PES Innov. Smart Grid Technol. Asia (ISGT)*, Perth, WA, Australia, pp. 1–6.

[40] A. Sarafi, G. Tsiropoulos, and P. Cottis, "Hybrid wireless-broadband over power lines: A promising broadband solution in rural areas," *IEEE Commun. Mag.*, vol. 47, no. 11, pp. 140–147, Nov. 2009.

[41] C. Paul, *Analysis of Multiconductor Transmission Lines*. Hoboken, NJ, USA: Wiley, 2008.

[42] X. Ding and J. Meng, "Channel estimation and simulation of an indoor power-line network via a recursive time-domain solution," *IEEE Trans. Power Del.*, vol. 24, no. 1, pp. 144–152, Jan. 2009.

Apostolos N. Milioudis (S'08) was born in Xanthi, Greece, in 1985. He received the Dipl.-Eng. and Ph.D. degrees in electrical and computer engineering from the Aristotle University of Thessaloniki, Thessaloniki, Greece, in 2007 and 2012, respectively.

His current research interests include power system protection and analysis, with special emphasis on the simulation of transmission and distribution systems, high impedance fault detection techniques, artificial intelligence applications in power systems, power line communications, and smart metering.

Georgios T. Andreou (S'98–A'02–M'08) was born in Thessaloniki, Greece, in 1976. He received the Dipl.-Eng. and Ph.D. degrees in electrical and computer engineering from the Aristotle University of Thessaloniki, Thessaloniki, in 2000 and 2006, respectively.

He is a Lecturer with the Department of Electrical and Computer Engineering, Aristotle University of Thessaloniki. His current research interests include power system analysis, with special emphasis on the simulation of transmission and distribution systems, electromagnetic and thermal field analysis, and PLCs.

Dimitris P. Labridis (S'88–M'90–SM'00) was born in Thessaloniki, Greece, in 1958. He received the Dipl.-Eng. and Ph.D. degrees in electrical and computer engineering from the Aristotle University of Thessaloniki, Thessaloniki, in 1981 and 1989, respectively.

Since 1990, he has been with the Electrical Engineering Department, Aristotle University of Thessaloniki, where he is currently a Professor. His current research interests include power system analysis, with special emphasis on the simulation of transmission and distribution systems.